

Quantitative proteomics unveils known and previously unrecognized alterations in neuropathic nerves

Victoria Defilippi¹ | Juli Petereit² | Valerie J. L. Handlos¹ | Lucia Notterpek¹ 

¹Department of Physiology and Cell Biology, School of Medicine, University of Nevada, Reno, Reno, Nevada, USA

²Nevada Bioinformatics Center (RRID:SCR_017802), University of Nevada, Reno, Reno, Nevada, USA

Correspondence

Lucia Notterpek, Department of Physiology and Cell Biology, School of Medicine, University of Nevada, Reno, 1664 N Virginia Street, Reno, NV, USA.
 Email: lnotterpek@unr.edu

Funding information

National Institutes of Health, Grant/Award Number: GM104944, P20GM130459 and GM103440

Abstract

Charcot–Marie–Tooth disease type 1E (CMT1E) is an inherited autosomal dominant peripheral neuropathy caused by mutations in the *peripheral myelin protein 22* (PMP22) gene. The identical leucine-to-proline (L16P) amino acid substitution in PMP22 is carried by the Trembler J (TrJ) mouse and is found in CMT1E patients presenting with early-onset disease. Peripheral nerves of patients diagnosed with CMT1E display a complex and varied histopathology, including Schwann cell hyperproliferation, abnormally thin myelin, axonal degeneration, and subaxonal morphological changes. Here, we have taken an unbiased data-independent analysis (DIA) mass spectrometry (MS) approach to quantify proteins from nerves of 3-week-old, age and genetic strain-matched wild-type (Wt) and heterozygous TrJ mice. Nerve proteins were dissolved in lysis buffer and digested into peptide fragments, and protein groups were quantified by liquid chromatography-mass spectrometry (LC-MS). A linear model determined statistically significant differences between the study groups, and proteins with an adjusted p-value of less than 0.05 were deemed significant. This untargeted proteomics approach identified 3759 quality-controlled protein groups, of which 884 demonstrated differential expression between the two genotypes. Gene ontology (GO) terms related to myelin and myelin maintenance confirm published data while revealing a previously undetected prominent decrease in peripheral myelin protein 2. The dataset corroborates the described pathophysiology of TrJ nerves, including elevated activity in the proteasome-lysosomal pathways, alterations in protein trafficking, and an increase in three macrophage-associated proteins. Previously unrecognized perturbations in RNA processing pathways and GO terms were also discovered. Proteomic abnormalities that overlap with other human neurological disorders besides CMT include Lafora Disease and Amyotrophic Lateral Sclerosis. Overall, this study confirms and extends current knowledge on the cellular pathophysiology in TrJ neuropathic nerves and provides novel insights for future examinations. Recognition of shared pathomechanisms across discrete neurological disorders offers opportunities

Abbreviations: AGC, automatic gain control; ALS, amyotrophic lateral sclerosis; CMT, Charcot–Marie–Tooth; CNS, central nervous system; DIA, data independent acquisition; G3BP1, stress granule assembly factor 1; GO, gene ontology; GFP, gas phase fractions; HCD, higher-energy collision dissociation; HNPP, hereditary neuropathy with pressure palsy; KEGG, Kyoto encyclopedia of genes and genomes; L16P, leucine-to-proline; LC-MS, liquid chromatography-mass spectrometry; MS, mass spectrometry; NF, neurofilament; PMP2, peripheral myelin protein 2; PMP22, peripheral myelin protein 22; PNS, peripheral nervous system; RRID, Research Resource Identifier; TrJ, Trembler J; Wt, wild-type.

This is an open access article under the terms of the [Creative Commons Attribution-NonCommercial-NoDerivs License](#), which permits use and distribution in any medium, provided the original work is properly cited, the use is non-commercial and no modifications or adaptations are made.

© 2024 The Author(s). *Journal of Neurochemistry* published by John Wiley & Sons Ltd on behalf of International Society for Neurochemistry.



for innovative disease-modifying therapeutics that could be effective for distinct neuropathies.

KEY WORDS

Charcot-Marie-Tooth, neuropathy, peripheral myelin protein 2, peripheral myelin protein 22, Trembler-J

1 | INTRODUCTION

Charcot-Marie-Tooth (CMT) diseases represent a heterogeneous group of inherited, progressive peripheral neuropathies. The largest fraction of demyelinating type 1 CMTs are associated with abnormal expression of the *peripheral myelin protein 22* (PMP22) gene (van Paassen et al., 2014). Duplication of the PMP22 gene causes CMT type 1A, while haploinsufficiency in PMP22 is linked with hereditary neuropathy with pressure palsy (HNPP) (DiVincenzo et al., 2014; Ekins et al., 2015; Fridman & Reilly, 2015). Missense mutations in PMP22 have also been identified to generate neuropathic phenotypes, ranging from severe early-onset disease to mild compression-induced neuropathies (Saporta et al., 2011). The identical spontaneous leucine-to-proline (L16P) substitution in the first transmembrane domain of the PMP22 protein is found within Trembler J (TrJ) mice and in human pedigrees with early-onset hereditary neuropathy (Suter et al., 1992; Valentijn et al., 1992). Therefore, TrJ mice represent a naturally occurring, well-characterized animal model for examining pathogenic mechanisms of PMP22-linked hereditary peripheral neuropathies and are the focus of the current study.

The L16P amino acid substitution in the first transmembrane domain of PMP22 affects the structure and subcellular trafficking of the hydrophobic protein, leading to cytosolic protein aggregation (Fortun et al., 2003; Sakakura et al., 2011). The misfolded protein impacts the ability of Schwann cells to differentiate and myelinate, resulting in thinly myelinated axons and nerve degeneration (Notterpek et al., 1997; Robertson et al., 1997). In mice, the homozygous L16P mutation in PMP22 is lethal by three weeks of age, and the cause for mortality is unknown (Notterpek et al., 1997). Cell culture studies with recombinant protein have shown a dominant negative effect of the mutant PMP22 on the wild-type (Wt) copy, with protein mistrafficking and retention in the Golgi (Tobler et al., 1999). Nerves from heterozygous mice display Schwann cell hypertrophy and macrophage infiltration, mimicking some of the histopathologies of human neuropathic nerves (Misko et al., 2002; Notterpek et al., 1997; Notterpek & Tolwani, 1999). The aggregated PMP22 impairs the proteasome's degradative capacity at a subcellular level, triggering enhanced autophagy-lysosomal pathway activity (Fortun et al., 2003). These previous studies indicate a complex subcellular response to the mutant PMP22, with multiple mechanisms involved.

Since TrJ mice model a human disorder, these animals have been used for therapeutic studies to slow or halt disease progression. Dietary approaches that have shown efficacy in improving nerve myelination and neuromuscular function of affected mice include supplementation

with curcumin, a neutral lipid-enriched high-fat diet, and an intermittent fasting regimen (Khajavi et al., 2007; Madorsky et al., 2009; Okamoto et al., 2013; Zhou et al., 2019). These studies illustrate plasticity and adaptation of neuropathic nerves to dietary modulation. Rapamycin, a small molecule activator of autophagy, was also tested in TrJ mice, and while this orally bioavailable drug improved nerve myelination, it failed to benefit neuromuscular performance likely due to the negative effect of rapamycin on protein synthesis within skeletal muscle (Nicks et al., 2014). TrJ mice have also been employed in gene therapy studies aiming to silence the mutant L16P-PMP22 allele by specific siRNAs, which enhanced motor function and improved nerve conduction velocity (Lee et al., 2017). Together, these studies indicate that TrJ mice serve as a suitable model for therapy testing; however, findings from these preclinical animal studies are yet to be translated to clinical applications. A comprehensive examination of the global protein changes within target nerve tissue is suited to benefit such efforts.

While the above cited studies have provided essential insights into the pathobiology caused by L16P-PMP22 mutation, a comprehensive, global proteomic view of affected nerves has not been described. Here, we compared the proteomic profile of sciatic nerves from 3-week-old, age- and strain-matched Wt and TrJ mice and identified previously recognized and unexamined pathways that differed between the two groups. Our study supports using unbiased bottom-up Data-independent acquisition (DIA) mass spectrometry-based proteomics for examining relevant tissues from complex disorders such as CMT1E.

2 | MATERIALS AND METHODS

2.1 | Experimental design and statistical rationale

We investigated the proteome of sciatic nerves from age-matched, genotyped Wt and TrJ ([RRID: MGI:5650998](#)) mice at postnatal day 21 (P21). At the time of weaning, the animals were separated from the dams and euthanized by CO₂ asphyxiation, followed by decapitation, which is consistent with the recommendations of the Panel of Euthanasia of the American Veterinary Medical Association. Until the weaning age, the pups were cohoused with the male and female parents in the same cage. At weaning age, the weight of the pups was around 10 g. Freshly-isolated nerves were frozen in liquid nitrogen and stored at -80°C until solubilization and subsequent analyses. Five biological replicates from Wt and TrJ mice were collected. Each sample included 2 nerves, left and right, from one individual mouse. Sex was collected but not considered a confounding factor and each group of five sample sets contained

nerves from 2 to 3 male and 2 to 3 female pups. The expression levels of the identified protein groups were compared via a generalized linear model to calculate differential abundance.

2.2 | Mouse model used

Breeder pairs of Wt and heterozygous TrJ mice on the C57/Bl6 (RRID:MGI:5650998) background were purchased from the Jackson Laboratory (Bar Harbor, ME) and housed in the University of Nevada animal care facilities, under specific pathogen-free (SPF) conditions, in ventilated cages. The mice had access to food and water ad libitum. Genotyping was performed on DNA isolated from tail biopsies of less than 10-day-old pups and determined by PCR (Notterpek et al., 1997). The University of Nevada, Reno Animal Care and Use Committee approved the use of animals for these studies (Protocol ID: 20-06-1013-1).

2.3 | Nerve protein preparation and digestion

Sciatic nerve proteins from individual samples (2 nerves per mouse, left and right) were solubilized with a RIPA lysis buffer 50 mM Tris-HCl (cat. no. 15568025), 150 mM NaCl (cat. no. FLBP35810), pH 7.2, with 1% deoxycholate (Sigma-Aldrich, cat. no. D6750), 0.5% NP40 (Sigma-Aldrich, cat. no. NP40S), 0.1% SDS (cat. no. 15553035), after crushing the tissue with a pestle under liquid nitrogen. Next, whole tissue protein lysates were rocked for 15 min at room temperature. Undissolved proteins were separated from the lysates by centrifugation at 12 000 rpm and were then dissolved in a 10 mM Tris-HCl with 3% SDS, and added to the previously dissolved protein solution (Fortun et al., 2003). The final combined lysates were sonicated, and protein content was determined using the bicinchoninic acid (Bio-Rad Laboratories) method. Next, 100 µg of each nerve lysate was reduced, alkylated with iodoacetamide, and digested with a trypsin/Lys-C protease mixture using a Thermo Scientific EasyPrep Mini MS Sample prep kit (cat. no. A40006), following manufacturer's recommendations. The trypsin/Lys-C was added 1:10 (enzyme: protein) for digestion. Samples were purified using the column supplied with the kit and separated by liquid chromatography.

2.4 | Liquid chromatography

Samples were analyzed using an UltiMate 3000 RSLC nano system (cat. no. ULTIM3000RSLCNANO; Thermo Scientific). The peptides were trapped before separation on a 300 µm i.d. × 5 mm C18 PepMap 100 trap (cat. no. 164946; Thermo Scientific) for 5 min at 10 µL/min. Separation was performed on a 50 cm uPAC C18 nano-LC column (cat. no. COL-CAP050G1B; PharmaFluidics) on an EasySpray source (cat. no. ES081; Thermo Scientific) fitted with a 30-µm ID stainless steel emitter (cat. no. 189351_-PepSep). Subsequent fractionation was performed at 350 nL/min using a gradient from 1% to 45% for 60 min (Solvent A 0.1%

Formic Acid, Solvent B Acetonitrile, 0.1% Formic Acid). The peptide sequence was determined by mass spectrometry (MS).

2.5 | Mass spectrometry (MS)

We performed data-independent analysis (DIA) using an Eclipse Tribrid Orbitrap mass spectrometer ([RRID:SCR_023618](#); Thermo Scientific) (Gillet et al., 2012). A chromatographic library was generated using the Spectronaut integrated database search engine Pulsar to create a hybrid using DIA and data-dependent analysis (DDA) spectra. The library was generated using six gas phase fractions (GPF) and full scan DDA of the biological sample pool. The GPF acquisition used 4 m/z precursor isolation windows in a staggered pattern (GPF1 398.4–502.5 m/z, GPF2 498.5–602.5 m/z, GPF3 598.5–702.6 m/z, GPF4 698.6–802.6 m/z, GPF5 798.6–902.7 m/z, GPF6 898.7–1002.7 m/z) at a resolution of 60 000, AGC target was set to custom with a normalized target of 1000%, maximum injection time was set to dynamic with a minimum of nine points across the peak, and an NCE of 33 using higher-energy collision dissociation (HCD). Three DDA full scan runs were performed on the biological pool. The MS precursor selection range was from 375 to 1500 m/z at a resolution of 120 K with a normalized automatic gain control (AGC) target of 250% and an automatic maximum injection time. Quadrupole isolation of 0.7 Th for MS² isolation and CID fragmentation in the linear ion trap with a collision energy of 35% and a 10 ms activation time. The MS² AGC was in standard mode with a 35 ms maximum injection time. The instrument was operated in a data-dependent mode with a 3-second cycle time and the most intense precursor priority. The dynamic exclusion was set to an exclusion duration of the 60 s with a 10 ppm tolerance. The test biological samples were run on an identical gradient as the GPFs using a staggered window scheme of 8 m/z over a mass range of 385–1015 m/z. Precursor isolation was performed in the Orbitrap at 60 000 resolution with a dynamic maximum injection, allowing for a minimum of nine points across the peak, a custom AGC normalized to 1000%, and an NCE of 33 using HCD. The species-specific FASTA database ([RRID:SCR_011819](#)) for Mouse (Mus musculus UP00000589_10090) containing 22 282 proteins and the known contaminants ([Crap_uniprot_with_human_MRSonbeadV2](#)) were downloaded from UniProt ([RRID:SCR_002380](#)). Variable modifications considered were: Carbamidomethylation C. Identification cut-offs for precursor and protein Q-value cutoffs were set to 0.01, and quantity was based on the area of MS² ions.

2.6 | Data analyses

Nonscaled, nontransformed intensity values were exported from Spectronaut 16 and analyzed with the statistical software R v4.2.1. Data underwent multiple quality assessment checks, e.g., poorly quantified proteins were omitted from the analysis, and replicated not well quantified were removed, i.e., many missing values within a sample. We also tested multiple transformation methods to determine the best scaling approach for this data. We confirmed the



overall data quality by principal component analysis and clustering the pairwise Pearson correlation coefficient. The data were transformed using the cyclic loess-log2 normalization before differential analysis with limma v3.52.4, which uses linear models to analyze the entire dataset and adjusts the model via empirical Bayes to infer information between proteins. *P*-values underwent a multiple testing correction using Benjamini-Hochberg, and the false discovery rate (adjusted *p*-value) was calculated to account for false positives. Here, proteins were deemed statistically significant with an adjusted *p*-value <0.05.

Protein IDs were mapped to gene names, and 3759 identifiers with their adjusted *p*-value and fold change were uploaded to iPathwayGuide (Advaita, Michigan) (07/25/2023). iPathwayGuide analyzes in the context of pathways obtained from the Kyoto Encyclopedia of Genes and Genomes (KEGG) database (Release 100.0+/11–12, Nov 21) (Kanehisa, 2002; Kanehisa & Goto, 2000), gene ontologies (GO) from the Gene Ontology Consortium database (2021-Nov4) (2001; Ashburner et al., 2000), and diseases from the KEGG database (Release 100.0+/11–12, Nov 21) (Kanehisa, 2002; Kanehisa & Goto, 2000).

2.7 | Nerve immunostaining

Sciatic nerves from P21 Wt and TrJ mice were flash-frozen in liquid nitrogen-cooled n-methyl butane (Sigma-Aldrich, cat. no. MX0760) and stored in liquid nitrogen until use. Samples were sectioned at 10 µm thickness and allowed to dry for 1 h, followed by rehydration and fixing in 4% paraformaldehyde (Electron Microscopy Sciences, cat. no. 15714) for 10 min and processed for immunolabeling. For anti-G3BP1 detection, after permeabilization with 0.1% Triton-X 100 (Sigma-Aldrich, cat. no. T8787) with 20 mM glycine (Sigma-Aldrich, cat. no. G8898) in phosphate-buffered saline (PBS), (pH: 7.2), blocking for nonspecific antibody binding was done at 22°C for 1 h in 20% normal goat serum (Sigma-Aldrich, cat. no. S26-M) in PBS, supplemented with 20 mM glycine (Sahoo et al., 2020). For Peripheral Myelin Protein 2 (PMP2) detection, the samples were similarly fixed, followed by permeabilization with 100% cold methanol at -20°C for 5 min (Hong et al., 2024). Primary antibodies against PMP2 (rabbit anti-PMP2; RRID:AB_2166978; 1:250), Ras GTPase-activating protein-binding protein 1 (G3BP1; rabbit anti-G3BP1; RRID:AB_1849348; 1:250), neurofilament (chicken anti-NF-M; RRID: AB_2572367, EnCor Biotechnology Inc) and lysosome-associated membrane protein 1 (LAMP1, RRID:AB_528127) were applied in blocking solution overnight at 4°C. Slides were then washed with PBS supplemented with 0.1% Tween and 20 mM glycine for four 30-min durations, followed by incubation in secondary antibodies (Abcam, goat anti-rabbit; RRID:AB_2650602, anti-chicken, cat.no. ab150169, or goat anti-rat, cat.no. 150157, each at 1:1k) at 22°C for 1 h. Coverslips were mounted with 90% glycerol in PBS and supplemented with 5 mg/mL propyl gallate (Sigma-Aldrich, cat. no. 02370). Slides were imaged on a Leica Stellaris 8 confocal microscope, and immunoreactivity was quantified by average fluorescent units within a specified area (PMP2 quantification 900 µm², G3BP1 quantification 225 µm²).

Six independent areas were measured from a single biological replicate ($n=3$ biological replicate per genotype) for PMP2, and measurements were taken randomly throughout the entire sciatic nerve cross section. For G3BP1, measurements were obtained throughout a 13000 µm² image. Final data points were normalized to the average Wt fluorescence to depict fold change. Statistical analyses and graphing were completed in GraphPad Prism 9. The immunostaining experiments were repeated on nerve samples from at least 5 independent mice, per genotype, and representative images are shown in the manuscript.

3 | RESULTS

3.1 | Data-independent analysis (DIA) of nerve samples from Wt and TrJ mice at a proteomic level

Hereditary peripheral neuropathies are progressive disorders with detectable abnormalities in affected nerves during early postnatal development (Fridman & Saporta, 2021). The P21 time point was chosen for our study, as at this age peripheral nerve myelination is largely complete in normal animals, providing a well-characterized reference point for analyses (Notterpek et al., 1997). Utilizing the LC-MS protein detection method allowed the identification of 3759 rigorously curated protein groups within the sciatic nerves of age-matched, mixed-sex wild-type (Wt) and heterozygous Trembler J (TrJ) mice. Based on their statistically significant differences and associated fold changes in expression, the proteins were subjected to pathway and gene ontology (GO) analyses.

During extensive quality control investigation of the DIA data, one of the Wt samples was identified as an outlier. This sample did not meet quality standards described in the methods section and was removed from further analyses. After removing low-quantified proteins, we retained 3759 quality-controlled protein groups. Thus, the resulting Wt ($n=4$) and TrJ ($n=5$) groups were used for subsequent comprehensive characterization. The principle component analysis of each sample indicates that the experimental groups separate on the first principle, accounting for 46% of the variation within the data (Figure 1a). Experimental groups were also confirmed by clustering the pairwise correlation coefficient of all samples (Figure 1b). Both measures validate that the disparity caused by genotypes is more significant than the biological variation across replicates. These data also indicate that the proteins behave differently across the two genotypes.

After validating the dataset's quality and normalization, we obtained 884 statistically significant differentially abundant proteins between TrJ and Wt. The volcano plot in Figure 2a represents each gene and its associated transformed fold-change and adjusted *p*-value. Specifically, 301 upregulated and 583 downregulated protein groups in TrJ, compared to Wt, contribute to enriched biological processes, cellular components, and molecular functions.

Next, the KEGG pathway and GO analyses (by Advaita iPathwayGuide software) were performed to understand the representation

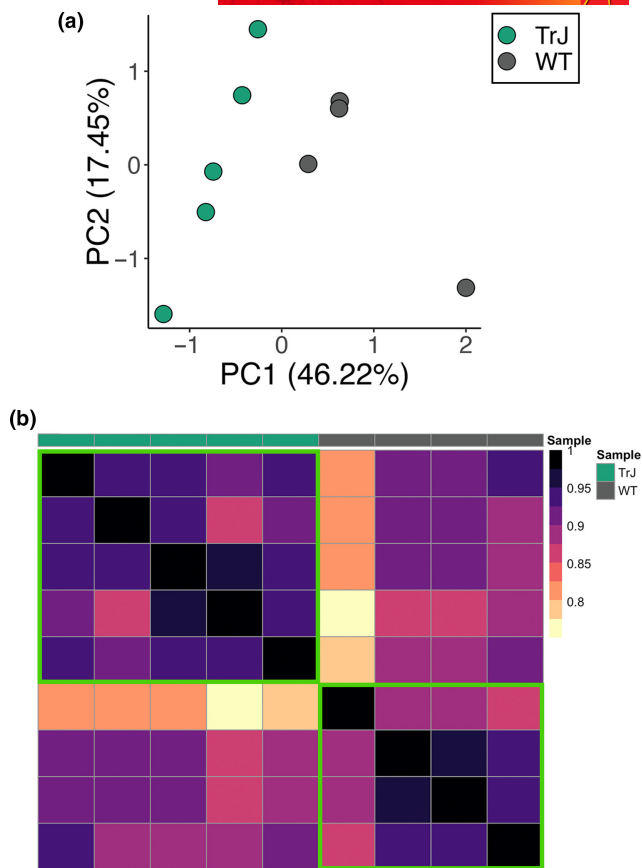


FIGURE 1 Experimental samples cluster by genotype (Wt and TrJ). (a) Graphical representation of a principal component analysis (PCA) between individual Wt ($n=8$ nerves, from 4 mice) and TrJ ($n=10$ nerves, from 5 mice) samples and genotypes. (b) Heatmap of pairwise correlation coefficients of experimental samples is shown. The color scale represents the Pearson correlation coefficient. Encased in the green boxes are the correlation values within a genotype.

of all differentially expressed proteins. Overrepresented KEGG pathways included the proteasome, spliceosome, and lysosome (Figure 2b). Other significantly affected pathways (i.e., Systemic lupus erythematosus, *Staphylococcus aureus* infection, and long-term potentiation KEGG pathways) were less relevant for the functioning of peripheral nerves, as these tissues do not contain neuronal cell bodies which are located in the spinal cord. Approximately 350 GO terms corresponding to biological processes, ~130 terms representing cellular components, and ~70 denoting molecular functions demonstrated significant enrichment from the differentially expressed protein pool (not shown). Of the top ten enriched biological processes, four are related to RNA metabolism, three to dopamine processing, and two are involved in axon development. One in macromolecule catabolic processing (Figure 2c). Enriched cellular components reflect the axonal changes within the sciatic nerves of neuropathic mice, with five out of the top ten GO terms correlating with nerve axon-related cellular components (Figure 2d). Additionally, nine of the top ten molecular functions enriched within the affected samples are associated with RNA and nucleic acid activities (Figure 2e). Based on these analyses, we further examined enriched

myelin and axonal gene products (Figures 3 and 4), as well as the top three augmented protein networks, namely the proteasome, lysosome, and spliceosome pathways (Figure 5–7).

3.2 | Differentially expressed proteins within CMT1E neuropathic mouse nerves unveil an overrepresentation of axonal constituents compared with glial myelin

PMP22, the disease-causing gene in the Trembler J CMT1E neuropathic model, is primarily expressed in myelin-forming Schwann cells (Snipes et al., 1992), yet among the study groups, out of the 884 differentially expressed genes, only 44 are related explicitly to myelin while 102 represent neuronal axons and 31 intersect between myelin and axon (Figure 3a). The protein groups found to be differentially expressed in all three categories (myelin, axon, and intersection) show no unidirectional change. There is a clear indication of up and downregulated protein groups throughout the myelin and axonal compartments of the neuropathic nerves (Figure 3b; Table 1). The importance of a bidirectional functional relationship between an axon and its myelin-forming glial cell is well established (Taveggia & Feltri, 2022) and is substantiated by this unbiased proteomic analysis. The results show that a disease originating in the glial cell disrupts the myelin proteome and impacts the axonal proteome to even a greater extent. There are almost three times as many differentially expressed axonal proteins as myelin proteins (Table 1), and the alterations between these axonal proteins show extensive complexity.

Among the identified myelin proteins, we found a 4.3-fold highly significant ($p < 0.001$) decrease in peripheral myelin protein 2 (PMP2) (Table 1), a gene that has yet to be examined in PMP22-linked neuropathies. In normal nerves, the PMP2 protein is concentrated around densely myelinated axons (Yim et al., 2022), and mutations in this cytosolic glial gene cause demyelinating neuropathies (Motley et al., 2016). In agreement, cross-sections of sciatic nerves from Wt mice display the characteristic mosaic distribution of PMP2-positive myelinated axons, identified by immunolabeling for NF-M (Figure 4a). Analysis of age-matched P21 TrJ mouse sciatic nerves is consistent with the proteomic data and shows an overall reduction PMP2-like reactivity around NF-positive axons (Figure 4b). In agreement, quantification from independent immunolabeling experiments reveals highly significant reduction in PMP2-like immunoreactivity in affected TrJ nerves (Figure 4c).

Regarding alterations in axonal constituents, the twofold increase in Stress Granule Assembly Factor 1 (G3BP1) (Table 1) was an unexpected finding. G3BP1 has been shown to limit nerve regeneration in the peripheral nervous system (PNS) (Sahoo et al., 2018), while in spinocerebellar ataxia, it lessened deficits (Koppapel et al., 2023). G3BP1 is a cytoplasmic protein which is distributed broadly within longitudinal nerve sections of 3-week-old Wt mice in regions that are also reactive for lysosomes, indicating cytosolic localization (Figure 4d). In samples from TrJ mice, an overall increase in G3BP1-like immunoreactivity is detected, often concentrated near Schwann cell nuclei

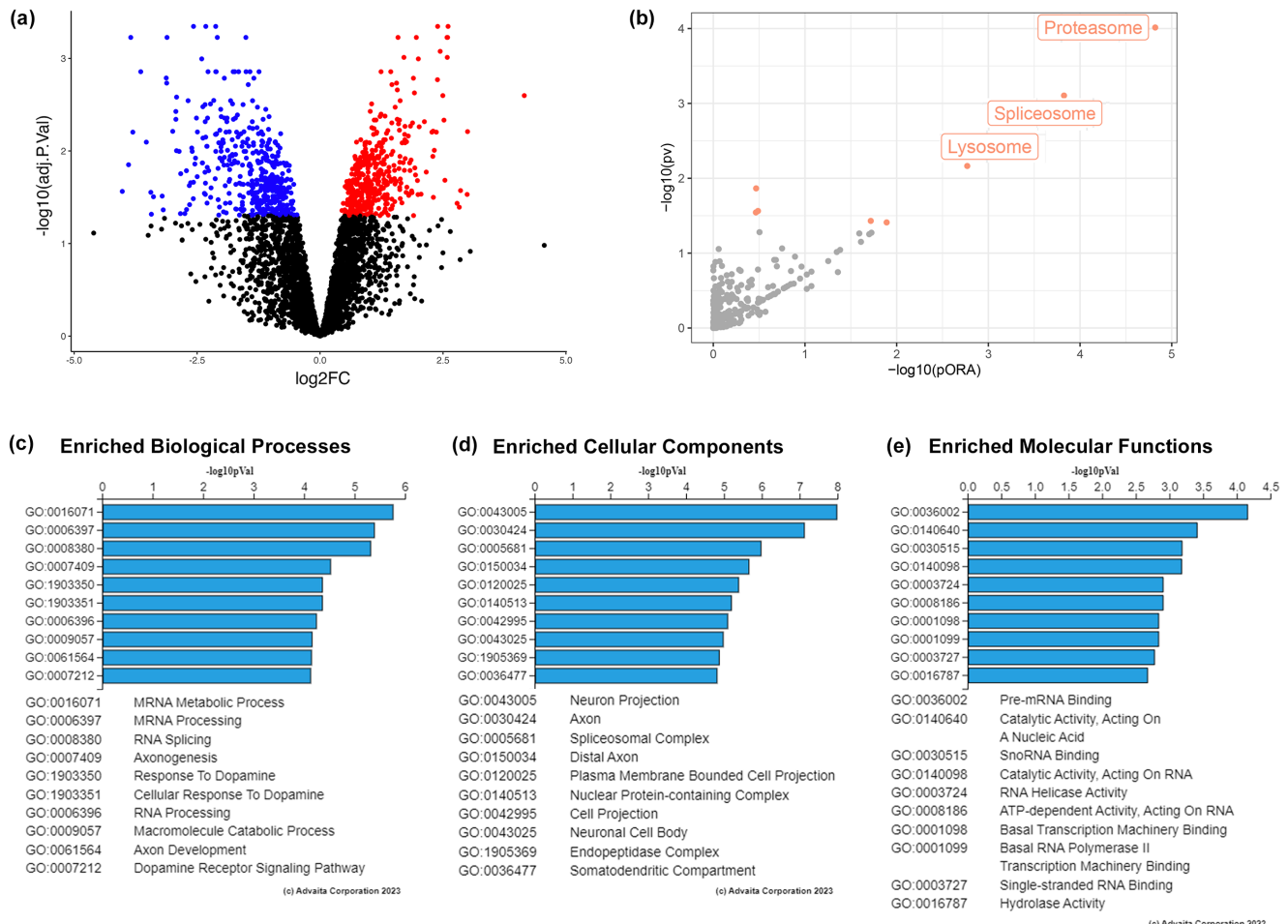


FIGURE 2 Over 800 proteins are differentially expressed in TrJ sciatic nerves compared to Wt. (a) Volcano plot representation of the 3759 recognized quality-controlled protein groups, of which 884 showed alteration between Wt ($n=8$ nerves, from 4 mice) and TrJ ($n=10$ nerves, from 5 mice) nerves: Statistically upregulated (red), downregulated (blue), and non-differentially expressed (black). (b) Detected overrepresentation and perturbation values within KEGG pathways are plotted. The pORA of the pathway caused by differentially expressed proteins is represented on the x-axis, and statistical significance is defined higher on the y-axis in orange. The top three overrepresented pathways are named on the plot. (c–e) The top ten significantly enriched biological processes, cellular components, and molecular functions are represented by the Gene Ontology (GO) term ID and associated transformed p-value.

(Figure 4e, arrowheads). While stress granules have not been studied in neuropathic peripheral glial cells, the granulation of G3BP1 has been investigated within the integrated stress response of oligodendrocytes (Chen et al., 2023; Hoch-Kraft et al., 2020). Here, for the first time we demonstrate the presence of G3BP1 within peripheral glial cells when their myelin is abnormal. Quantification of G3BP1-like immunoreactivity from independent nerve samples confirms elevated expression in affected nerves (Figure 4f), as indicated in Table 1.

3.3 | Proteomic profiling confirms and extends known disturbances in subcellular degradative pathways and the inflammatory response

Previously, we described the presence of PMP22 protein aggregates and upregulation of the ubiquitin-proteasome and autophagy-lysosomal pathways in nerves of TrJ mice (Fortun et al., 2003;

Notterpek et al., 1997). In accord, the KEGG pathway representing the mouse proteasome distinguishes 47 proteins known to be annotated to the proteasome in the corresponding literature. Of the 37 proteasomal protein peptide signatures identified within the nerves of TrJ mice, 21 are differentially expressed. Those with differential expressions cause a disturbance in the subunit composition of the proteasome (Figure 5a). The overproduced proteins are known to interact, creating the proteasomal complex, and are regulated by the single reduced protein, the proteasome inhibitor subunit 1 (Figure 5b). The elevated expression of proteins encompassing each subunit of the proteasome suggests an attempt to enhance proteolysis within affected neuropathic nerves.

As protein degradative mechanisms are co-regulated by the transcription factor EB (Napolitano & Ballabio, 2016), it is predictable that our analyses also distinguished perturbations in the lysosomal pathway (Figure 6). This finding agrees with our previous report, where traditional western blotting showed increased expression of

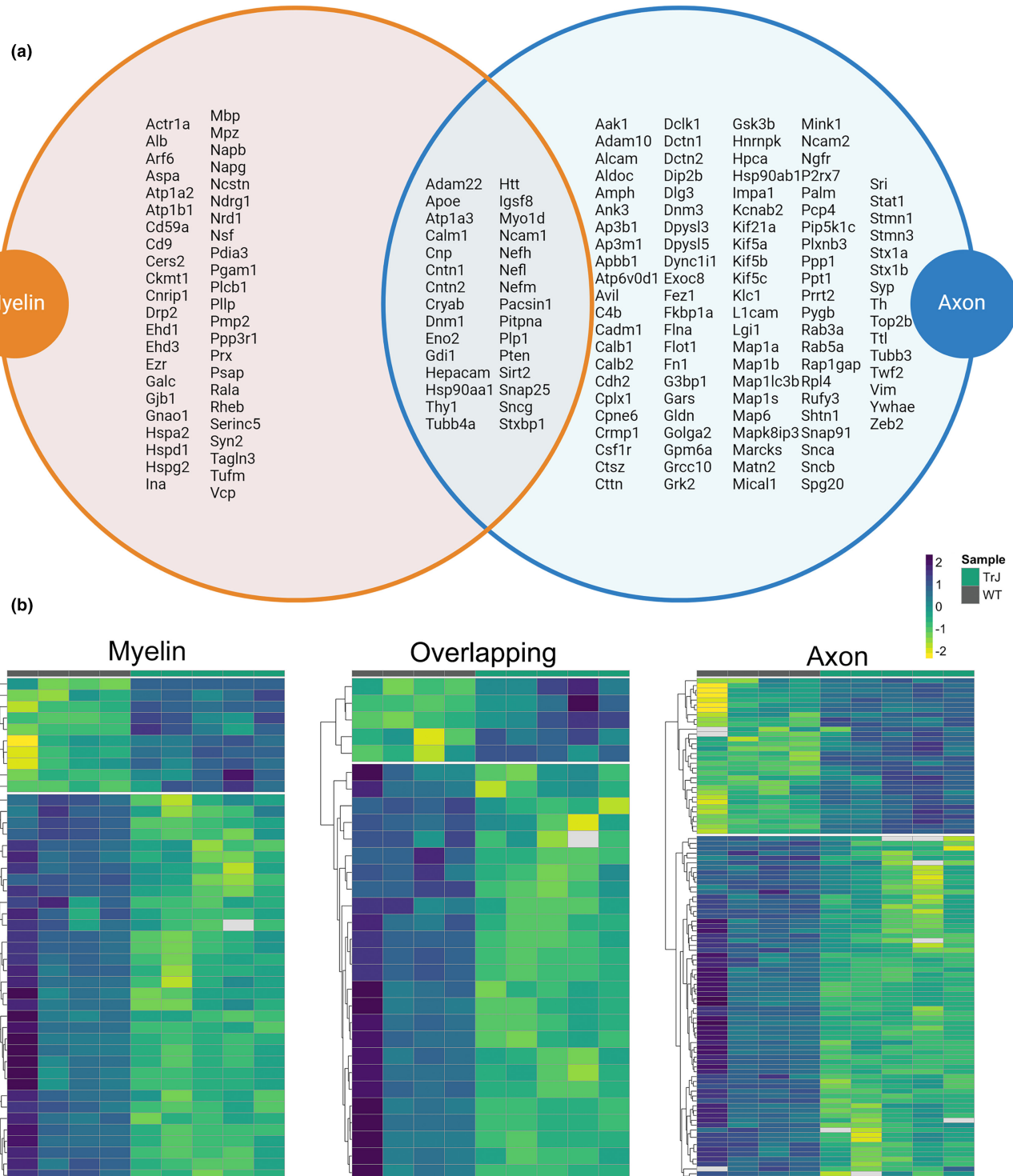


FIGURE 3 Analyses of sciatic nerve proteins reveal deficits in the myelin and axonal proteomes of affected neuropathic mice. (a) Venn diagram depicting differentially expressed protein groups within TrJ ($n=10$ nerves, from 5 mice), compared with Wt ($n=8$ nerves, from 4 mice) sciatic nerves. Indicated proteins are mapped to axonal (blue), myelin (orange), or overlapping groups, with axonal and myelin gene ontology (GO) terms. Created with BioRender.com. (b) Heatmaps showing differential expression of each protein group within each section of the Venn diagram and log2fold-change in expression levels are represented by the Viridis color scale. The rows are shown by standard hierarchical clustering.

lysosome-associated membrane protein 1 (LAMP1) and cathepsins in TrJ neuropathic nerves (Notterpek et al., 1997). One hundred thirty-five protein groups are annotated to the mouse lysosomal KEGG

pathway, and 48 protein signatures are picked up within the analyzed nerves. Neuropathic nerves present with 21 differentially expressed protein groups altering the lysosomal pathway. The differentially

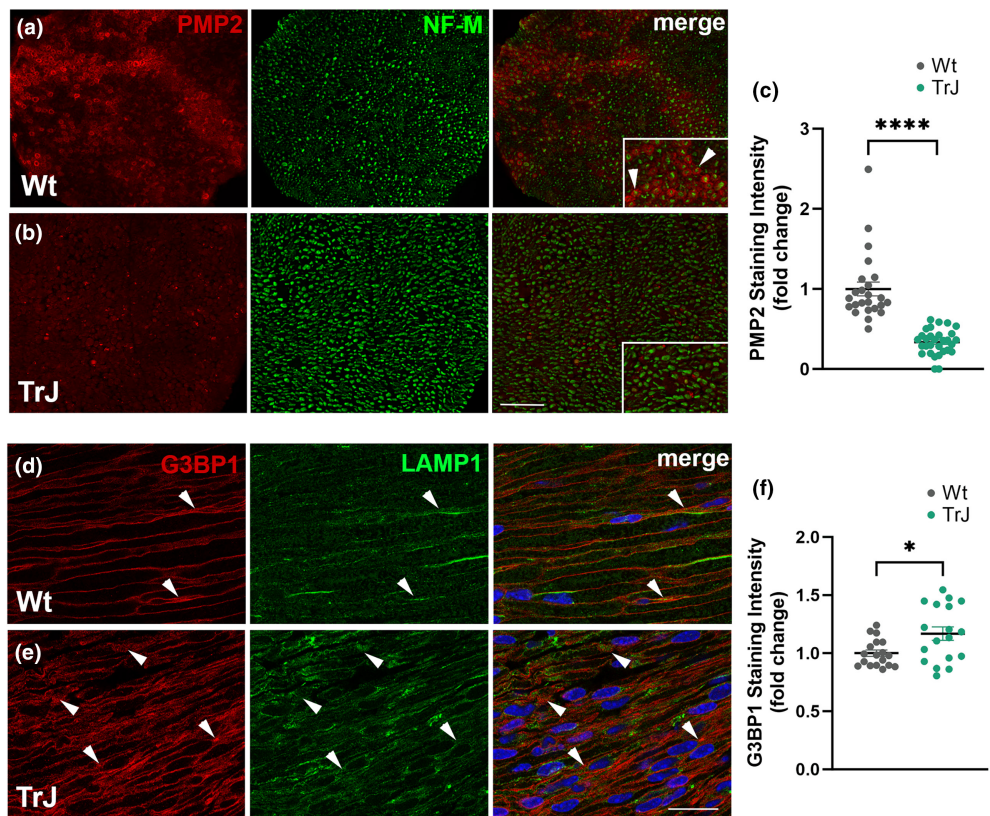


FIGURE 4 Immunolabeling corroborates alterations in PMP2 and G3BP1 in affected sciatic nerves. (a, b) Double immunostaining of cross sections of Wt (a) and TrJ (b) sciatic nerves, independent of the proteomic nerve set, for the detection of peripheral myelin protein 2 (PMP2, red) NF-M (green). On the merged image, myelinated axons appear as NF-M labeled axons, surrounded by round PMP2-reactive myelin (arrows in image in lower right corner). (c) Quantification from six independent $900\text{ }\mu\text{m}^2$ areas of entire sciatic nerve cross sections of each genotype ($n=3$ biological replicates). (d, e) Longitudinal nerve sections from Wt (d) and TrJ (e) mice, independent of the proteomic tissue samples, identifies elevated G3BP1-like immunoreactivity (red) in subcellular compartments that are reactive for lysosomes (LAMP1, green). On single plane confocal images arrowheads mark prominent G3BP1-reactive areas that are seen near Hoechst dye labeled glial nuclei (arrowheads). Images shown are representative of $n>5$ independent immunolabeling experiments, each containing nerves from distinct mice. (f) Fold-change depiction of $n=5$ biological replicates from each genotype and six independent $225\text{ }\mu\text{m}^2$ areas, quantified within a $13000\text{ }\mu\text{m}^2$ image. Unpaired student's t-test, Welch correction. * $p<0.05$, *** $p<0.0001$. Scale bars, $50\text{ }\mu\text{m}$ (b) and $25\text{ }\mu\text{m}$ (e).

expressed proteins mainly trend toward overexpression, with 18 upregulated molecules, ranging with a log₂ fold change of -1.6 to 1.9 (Figure 6a). Several proteins are binding partners, and a few are known to react. Cathepsin C, the most highly upregulated protein in the pathway, is a catalyst for protein–protein interaction (not explicitly shown) (Figure 6b). Together, the pronounced enhancement in proteins representing degradative mechanisms is hypothesized to reflect the attempt of the neuropathic nerves to repair the abnormal myelin (Zhou & Notterpek, 2016).

Previous studies have shown adult TrJ mouse nerves have an increased presence of macrophages, while young and adult nerves both express signaling molecules linked with the inflammatory response (Misko et al., 2002; Okamoto et al., 2013). This proteomic study supports these findings in affected nerves, as revealed by elevation of the macrophage cell surface receptor CD44 (log₂fc 0.67, adjusted p-value 0.0352). Further, two regulators of inflammation due to immune reactions, MEFV and P2RX7 (Adinolfi et al., 2018; Krainer et al., 2020), are significantly downregulated within affected nerve samples, as compared with age-matched Wt (Table 2).

3.4 | Enrichment of the spliceosomal pathway and the relation of the TrJ neuropathy to other neurodegenerative disorders

The unbiased proteomic approach allowed us to discover previously unrecognized perturbations in neuropathic nerves (Figure 7). While splicing defects have been studied in central nervous system (CNS) neurodegenerative disorders (Li et al., 2023), their role in peripheral neuropathies has not been thoroughly explored. As shown in Figure 7, 180 database genes are recognized to be annotated to the spliceosomal KEGG pathway. Seventy-four of those protein groups have recorded values from the analyzed nerves, with 32 differentially expressed and exclusively upregulated. The upregulation of the differential proteins is seen throughout the entire pathway (Figure 7). Within the 884 differentially expressed protein groups of the TrJ samples, 167 proteins are represented within GO terms related to RNA synthesis and its processing. Perturbation of the spliceosomal pathway in affected nerves is in part likely the reflection of mRNA processing events within neuropathic glial cells that contain protein

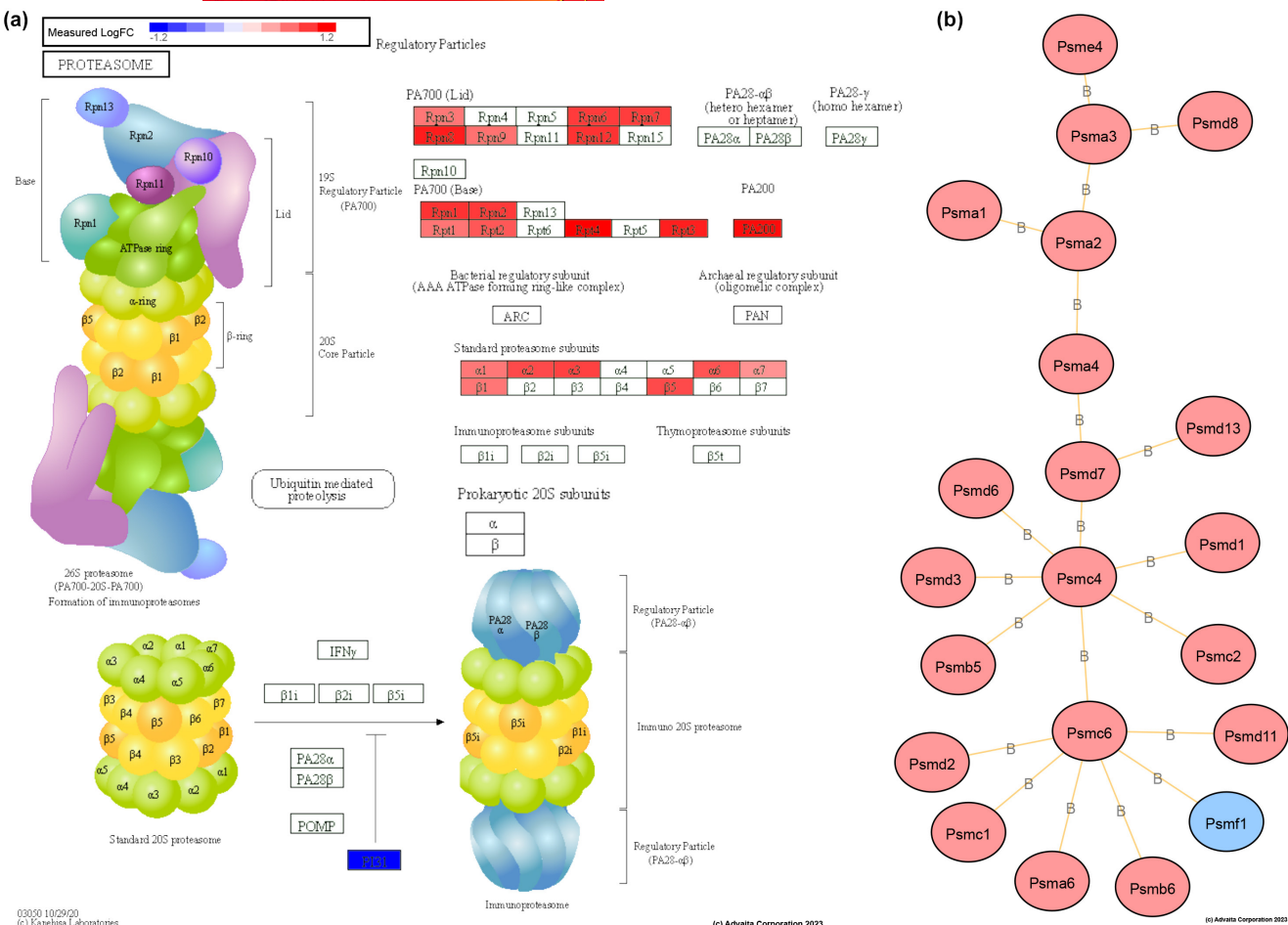


FIGURE 5 Nerve proteome from neuropathic mice reveals pathway variations affecting protein degradation and trafficking. (a) The proteasomal KEGG pathway is shown with corresponding log₂ fold-change (red: Upregulated, blue: Downregulated) of differentially expressed proteins with an adjusted *p*-value <0.05. (b) Network analyses depicting the mechanistic reaction between differentially expressed proteins in the pathway. Yellow lines with a B represent binding proteins, red indicates the upregulated, and blue signifies downregulated genes in Trj samples (*n*=10 nerves, from 5 mice), as compared with Wt (*n*=8 nerves, from 4 mice).

aggregates (Fortun et al., 2003; Notterpek, Snipes, & Shooter, 1999; Tobler et al., 1999; Zhou et al., 2020). Furthermore, enrichment of the spliceosome occurs in cancers and is known as a driver of cell proliferation (Karamysheva et al., 2015; Yoshimi & Abdel-Wahab, 2017). Accordingly, in affected TrJ nerves, at three weeks of postnatal development, the Schwann cells fail to differentiate and continue to divide (Notterpek et al., 1997), which is incompatible with proper myelination.

Given the upregulation of previously unrecognized subcellular mechanisms in the neuropathic nerves, we investigated the commonality of these perturbations among other human disorders ([Figure 8](#)). Approximately 30 diseases are related to the differentially expressed protein groups of the neuropathic nerves. These diseases range between the groupings of endocrine and nutritional, congenital and chromosomal abnormalities, and nervous system diseases ([Figure 8a](#)). We chose to focus on nervous system disorders due to their relevance to the current study. Neurological diseases identified include illnesses of the myoneural junction and muscle, systemic atrophies of the CNS, episodic and paroxysmal disorders, and polyneuropathies of

the PNS ([Figure 8b](#)). [Figure 8c](#) depicts the top six neural disorders (A-F), which share overlapping protein perturbations with the neuropathic nerves, and the specific proteins corresponding to the disease are represented in the chord diagram. As expected, CMT is the most enriched nervous system disease, while there are parallels with other illnesses as well. For example, TrJ mouse nerves display abnormal accumulation of cellular products in the cytoplasm ([Fortun et al., 2003](#); [Zhou et al., 2020](#)), similar to neuronal ceroid lipofuscinosis, which represents a group of neurodegenerative diseases characterized by undegraded lysosomal cargo ([Nita et al., 2016](#)). CMT1E mouse nerves also share similarities with Lafora disease, which is characterized by an accumulation of glycogen-derived particles, termed Lafora bodies, due to a dysfunction in the ubiquitin-proteasome and autophagy pathways ([Fortun et al., 2003](#); [Mitra et al., 2022](#)).

In addition, disorders unrelated to protein degradative mechanisms were also identified, including periventricular nodular heterotopia and complex cortical dysplasia, which are brain malformations due to defects in neuronal migration and disturbed axonal guidance within the cerebrum or cerebral cortex caused by changes in cytoskeletal

**TABLE 1** Differentially expressed protein groups within TrJ sciatic nerves corresponding to myelin and axonal compartments.

Group	Gene	log2FC	Pval
Myelin	Actr1a	-0.63	0.0144
Myelin	Alb	0.75	0.0364
Myelin	Arf6	-0.91	0.025
Myelin	Aspa	-1.25	0.0065
Myelin	Atp1a2	-0.57	0.0417
Myelin	Atp1b1	-0.88	0.0344
Myelin	Cd59a	-3.39	0.0312
Myelin	Cd9	-2.51	0.0044
Myelin	Cers2	-0.94	0.0217
Myelin	Ckmt1	-0.98	0.0134
Myelin	Cnrip1	-0.91	0.0488
Myelin	Drp2	-3.13	0.0016
Myelin	Ehd1	-0.97	0.0254
Myelin	Ehd3	-1.1	0.0213
Myelin	Ezr	1.14	0.0142
Myelin	GalC	-0.83	0.0275
Myelin	Gjb1	-2.34	0.0032
Myelin	Gnao1	-1.2	0.0062
Myelin	Mpz	-1.72	0.0044
Myelin	Napb	-1.21	0.0342
Myelin	Napg	-0.82	0.0388
Myelin	Ncstn	1.36	0.0114
Myelin	Ndrg1	-0.68	0.0136
Myelin	Nsf	-0.81	0.0492
Myelin	Pdia3	0.93	0.0392
Myelin	Pgam1	-1.08	0.0425
Myelin	Plcb1	-2.01	0.0101
Myelin	Pllp	-2.01	0.0043
Myelin	Pmp2	-2.11	0.0014
Myelin	Ppp3r1	-2.3	0.0089
Myelin	Prx	-1.57	0.008
Myelin	Psap	1.31	0.0138
Myelin	Rala	-1.83	0.0114
Myelin	Rheb	-1.55	0.0062
Myelin	Serinc5	1.92	0.0024
Myelin	Syn2	-0.89	0.0449
Myelin	Tagln3	-1.74	0.0128
Myelin	Tufm	0.69	0.0295
Myelin	Vcp	0.67	0.0261
Myelin	Hspd1	0.55	0.023
Myelin	Hspg2	0.77	0.0294
Myelin	Ina	-1.37	0.0226
Axon	Aak1	-0.96	0.0214
Axon	Adam10	-0.75	0.0308
Axon	Alcam	-0.87	0.0191
Axon	Aldoc	-1.59	0.0089

TABLE 1 (Continued)

Group	Gene	log2FC	Pval
Axon	Amph	-1.19	0.0131
Axon	Ank3	-0.67	0.0201
Axon	Ap3b1	0.99	0.0124
Axon	Ap3m1	0.67	0.0274
Axon	Apbb1	-1.55	0.043
Axon	Atp6v0d1	0.67	0.022
Axon	Avil	-0.98	0.0248
Axon	C4b	0.76	0.0402
Axon	Cadm1	-1.28	0.0056
Axon	Calb1	-2.49	0.0062
Axon	Calb2	-2.6	0.0101
Axon	Cdh2	-1.14	0.0317
Axon	Cplx1	-2.92	0.0026
Axon	Cpne6	-1.36	0.0228
Axon	Crmp1	-0.67	0.0384
Axon	Csf1r	1.87	0.0282
Axon	Ctsz	1.73	0.0121
Axon	Cttn	1.23	0.0082
Axon	Dclk1	0.94	0.0229
Axon	Dctn1	-0.59	0.0205
Axon	Dctn2	-0.86	0.0087
Axon	Dip2b	0.62	0.0466
Axon	Dlg3	1.3	0.0076
Axon	Dnm3	-1.13	0.0483
Axon	Dpysl3	-1.09	0.0126
Axon	Dpysl5	-1.16	0.0162
Axon	Dync1i1	-2.16	0.0028
Axon	Exoc8	-1.89	0.0044
Axon	Fez1	-2.87	0.0101
Axon	Fkbp1a	-1.35	0.0299
Axon	Flna	0.71	0.0275
Axon	Flot1	-0.85	0.0103
Axon	Fn1	1.16	0.0206
Axon	G3bp1	1.01	0.0141
Axon	Gars	-0.8	0.0222
Axon	Gldn	2.44	8.00E-04
Axon	Golga2	1.39	0.0493
Axon	Gpm6a	-3.21	0.0307
Axon	Grcc10	-1.42	0.017
Axon	Grk2	-0.82	0.0492
Axon	Gsk3b	-1.07	0.0268
Axon	Hnrnpk	0.85	0.0492
Axon	Hpc1	-0.91	0.008
Axon	Hsp90ab1	0.72	0.0486
Axon	Impa1	-0.82	0.0254
Axon	Kcnab2	-1.97	0.0082

TABLE 1 (Continued)

Group	Gene	log2FC	Pval
Axon	Kif21a	-1.06	0.0214
Axon	Kif5a	-2.01	0.0091
Axon	Kif5b	-0.66	0.0475
Axon	Kif5c	-1.05	0.0058
Axon	Klc1	-0.8	0.0065
Axon	L1cam	-1.1	0.0109
Axon	Lgi1	-1.58	0.0384
Axon	Map1a	-0.93	0.015
Axon	Map1b	-0.87	0.0245
Axon	Map1lc3b	-0.68	0.0264
Axon	Map1s	0.53	0.0246
Axon	Map6	-1.21	0.0268
Axon	Mapk8ip3	-1.88	0.0142
Axon	Marcks	-1.91	0.0466
Axon	Matn2	1.17	0.0114
Axon	Mical1	0.94	0.0104
Axon	Mink1	0.73	0.0203
Axon	Ncam2	-0.98	0.0236
Axon	Ngfr	1.1	0.2301
Axon	P2rx7	-1.39	0.016
Axon	Palm	-1.72	0.0089
Axon	Pcp4	-2.12	0.0014
Axon	Pip5k1c	-1.84	0.0203
Axon	Plxnb3	0.85	0.0323
Axon	Ppt1	0.72	0.0122
Axon	Prrt2	-2.07	0.0154
Axon	Pygb	-0.98	0.0235
Axon	Rab3a	-0.75	0.0296
Axon	Rab5a	-1.21	0.0205
Axon	Rap1gap	1.56	0.0018
Axon	Rpl4	1	0.0378
Axon	Rufy3	-1.43	0.0138
Axon	Shtn1	2.5	0.0025
Axon	Snap91	-1.99	0.0128
Axon	Snca	-1.79	0.0113
Axon	Sncb	-1.57	0.0032
Axon	Sri	-0.7	0.0457
Axon	Stat1	0.93	0.0082
Axon	Stmn1	-2.1	0.0065
Axon	Stmn3	-0.94	0.0236
Axon	Stx1a	-1.92	0.0368
Axon	Stx1b	-1.9	0.0048
Axon	Syp	-2.05	0.0403
Axon	Th	-2.13	0.0066
Axon	Top2b	1.1	0.0338
Axon	Ttl	-1.06	0.0205
Axon	Tubb3	-1.02	0.0255

TABLE 1 (Continued)

Group	Gene	log2FC	Pval
Axon	Twf2	0.56	0.0352
Axon	Vim	0.97	0.0123
Axon	Ywhae	-0.54	0.0425
Axon	Zeb2	0.95	0.0483
Both	Adam22	-1.5	0.0082
Both	Apoe	1.71	0.0162
Both	Atp1a3	-1.66	0.0014
Both	Calm1	-0.79	0.0276
Both	Cnp	-0.81	0.0093
Both	Cntn1	-1.38	0.021
Both	Cntn2	-1.83	0.0364
Both	Cryab	0.69	0.0376
Both	Dnm1	-1.64	0.0067
Both	Eno2	-1.6	0.0227
Both	Gdi1	-0.91	0.0116
Both	Hepacam	-1.05	0.0128
Both	Hsp90aa1	0.56	0.049
Both	Thy1	-0.91	0.0498
Both	Tubb4a	-1.03	0.0197
Both	Htt	0.83	0.0248
Both	Igfsf8	-0.64	0.0163
Both	Myo1d	-2.61	0.0093
Both	Ncam1	-0.59	0.0284
Both	Nefh	-1.4	0.0236
Both	Nefl	-1.2	0.0241
Both	Nefm	-1.15	0.0206
Both	Pacsin1	-2.04	0.0119
Both	Pitpna	-1	0.019
Both	Plp1	-2.04	0.006
Both	Pten	0.99	0.0405
Both	Sirt2	-1.74	0.0014
Both	Snap25	-2.83	0.0176
Both	Sncg	-1.85	0.0287
Both	Stxbp1	-1.12	0.0196

mechanisms (Khoo et al., 2020; Klingler et al., 2021). Recognizing perturbations in subcellular cytoskeletal networks in CMT1E neuropathic nerves is an additional novel finding, likely a reflection of abnormal myelination and altered axo-glial communications (Robertson et al., 1997). Furthermore, the protein abnormalities in CMT1E mouse nerves relate highly with amyotrophic lateral sclerosis (ALS), also known as Lou Gehrig's disease, which is considered a disorder of CNS motor neurons and does involve proteostatic imbalance (Cicardi et al., 2021). CMT and ALS have been investigated for overlapping pathophysologies, including comparison of nerve degeneration by ultrasound (Hildebrand et al., 2023). While the TrJ mouse is used to study CMT1E neuropathy, these results suggest that this spontaneous animal model could be valuable for investigating various therapeutic targets.

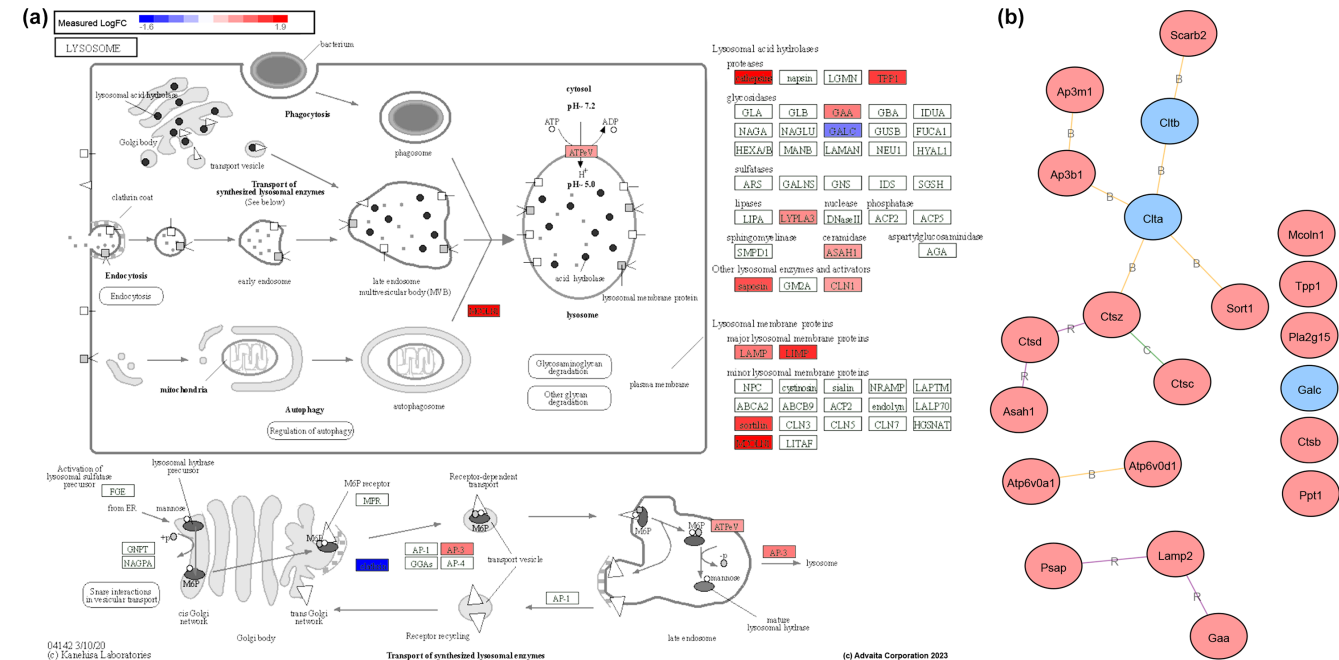


FIGURE 6 Differentially expressed proteins within the lysosomal pathway of sciatic nerves from TrJ mice. (a) The lysosomal KEGG pathway is depicted with corresponding differentially expressed proteins (blue: Downregulated, red: Upregulated). (b) The mechanistic network analysis of the differential proteins shows upregulated (red) and downregulated (blue) proteins and their regulatory interactions: Purple lines with an R indicate proteins that react with each other, green lines with a C are protein catalysts and yellow lines with a B represent protein binding. Data shown was derived from the proteome of Wt ($n=8$ nerves, from 4 mice) and TrJ ($n=10$ nerves, from 5 mice) mice.

TABLE 2 Macrophage-specific proteins associated with the biological process, inflammatory response [GO:0006954].

Gene ID	log2 FC	Adj p-value
C5	0.35	0.2071
Cd44	0.67	0.0352
Akt1	-0.04	0.8975
Mif	-0.24	0.5551
Thbs1	0.5	0.3819
Itgav	0.27	0.3392
Mapkapk2	0.37	0.4037
Hmgb1	0.47	0.1502
Nfix	0.55	0.5639
Pja2	0.45	0.6968
Mefv	-2.12	0.0066
P2rx7	-1.39	0.016
Stk39	-0.41	0.1458

Note: The proteins with significant change are shown in green.

4 | DISCUSSION

The described comprehensive proteome analyses of Wt and neuropathic nerves from 3-week-old mice provide insights into the global molecular changes triggered by the mutated PMP22. The proteomic phenotypes demonstrate distinct experimental clusters, with more than 800 protein groups differentially expressed between the affected and unaffected samples. The neuropathic genotype enriched

hundreds of GO terms and pathways, uncovering pronounced enrichment in the axonal compartment compared with myelin. Peripheral nerves from TrJ mice demonstrate a reduced amount and altered mosaicism of PMP2 in their myelin and heightened stress granule assembly, as indicated by clumping of G3BP1. Furthermore, previously investigated degradative mechanisms, including the proteasomal and lysosomal pathways, are notably enriched within affected nerves, corroborating published studies (Fortun et al., 2003; Notterpek et al., 1997). This unbiased approach also revealed new mechanisms contributing to the neuropathic disease phenotype, namely the slipeosome and RNA processing pathways.

To date, limited studies have addressed global changes in the proteome of neuropathic nerves. The first comprehensive report specifically examined differences in myelin between healthy and periaxin-deficient neuropathic mice (Siems et al., 2020). This study aimed to develop a workflow to analyze myelin, a unique subcellular structure critical for normal nervous system functions. As planned, these scientists established an adaptable workflow for future analyses and identified 32 neuropathy-causing molecules, some previously unrecognized within myelin. Another study successfully applied proteomics to investigate the pathophysiology in neuropathic patients with mutations in aminoacyl tRNA-synthetase (Hoyer et al., 2022). By analyzing the proteome of peripheral blood mononuclear cells, they uncovered inflammation and mitochondrial dysfunction as contributing factors in disease progression. A recent study has taken a different approach and compared the proteome of peripheral nerves from three-month-old CMT1A rats with samples from nerve crush injuries (Msheik et al., 2023). The main findings from this report include the

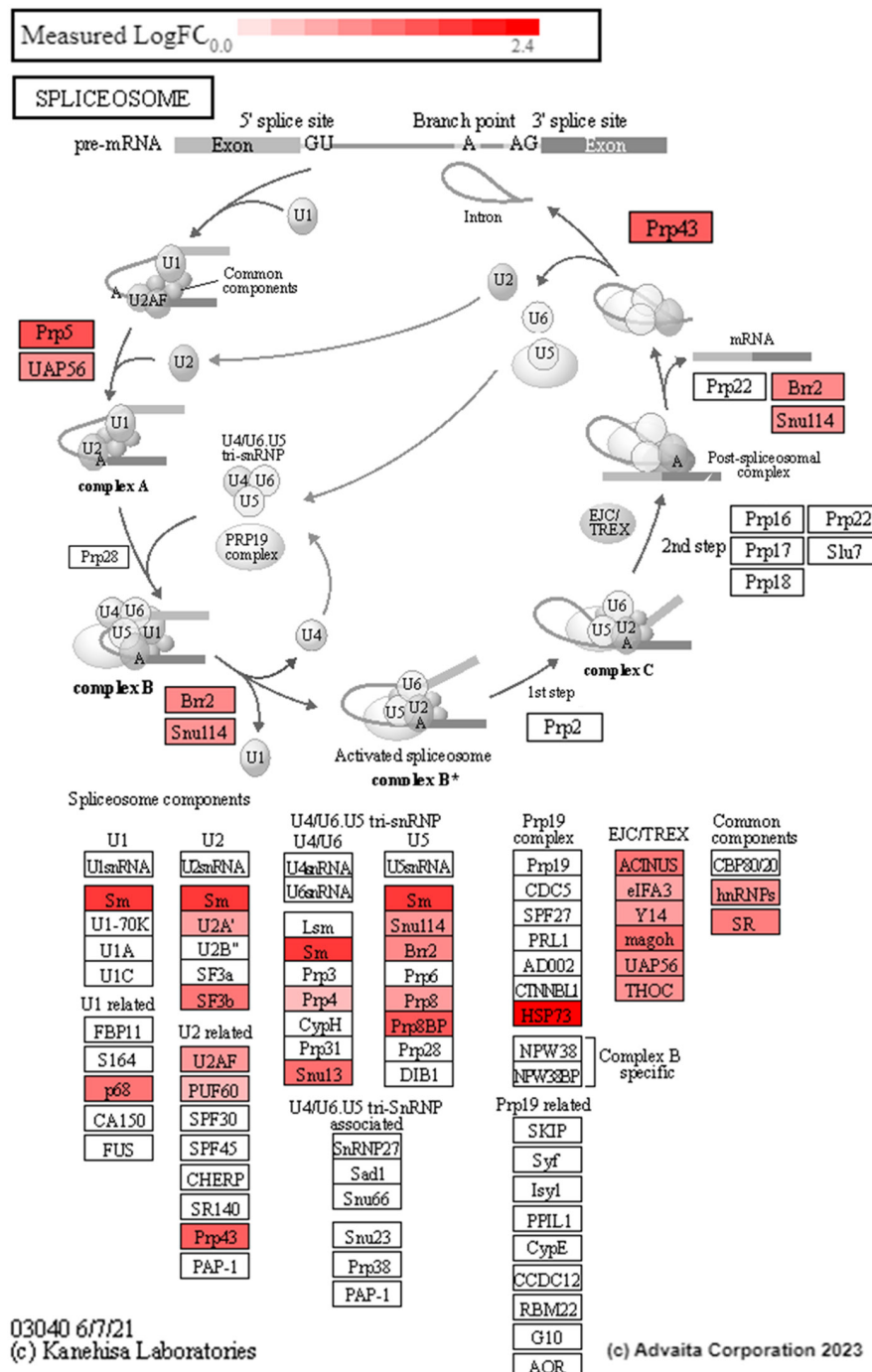


FIGURE 7 Enrichment in RNA processing cellular functions is the most differentially expressed gene ontology in sciatic nerves of TrJ mice. Spliceosome KEGG pathway is depicted with corresponding differential proteins colored by magnitude of log₂fold-change (red: Upregulated). Data shown represents the proteome of 3-week-old Wt ($n=8$ nerves, from 4 mice) and TrJ ($n=10$ nerves, from 5 mice) mice.

oxidative stress pathway, a common mechanism between post-acute nerve injury and symptomatic hereditary neuropathy in three-month-old animals. In comparison, our proteomic DIA of young neuropathic nerves uncovers early events in the disease cascade from a spontaneous, non-transgenic animal model of CMT1E.

The tissue source and the specific analyzed starting material are important considerations when designing and interpreting data from a proteomic study. We chose segments of the sciatic nerve, which contain Schwann cells, endoneurial cells, axons, and some cells from the vasculature, but no neuronal cell bodies. This approach allowed us to identify pronounced changes in axonal proteins, an important aspect for understanding the pathophysiology of peripheral

neuropathies, which can be distinguished as type 1, glial-, or type 2, axonal-origin (El-Abassi et al., 2014). As described in Figures 3 and 4, we uncovered pronounced alterations in the axonal compartment, along with the predicted abnormalities in myelin proteins. These results are supported by early findings in the Trembler model, where changes in axonal caliber were some of the first described morphological modifications (de Waegh & Brady, 1990; de Waegh et al., 1992). A newly-recognized altered myelin protein, PMP2 resides in glial cells surrounding large caliber axons (Yim et al., 2022), with its dysfunction causing type 1 neuropathy (Hong et al., 2016; Motley et al., 2016). G3BP1 has been linked with type 2 neuropathy (Cui et al., 2023), yet was also distinguished here in a type 1 disease

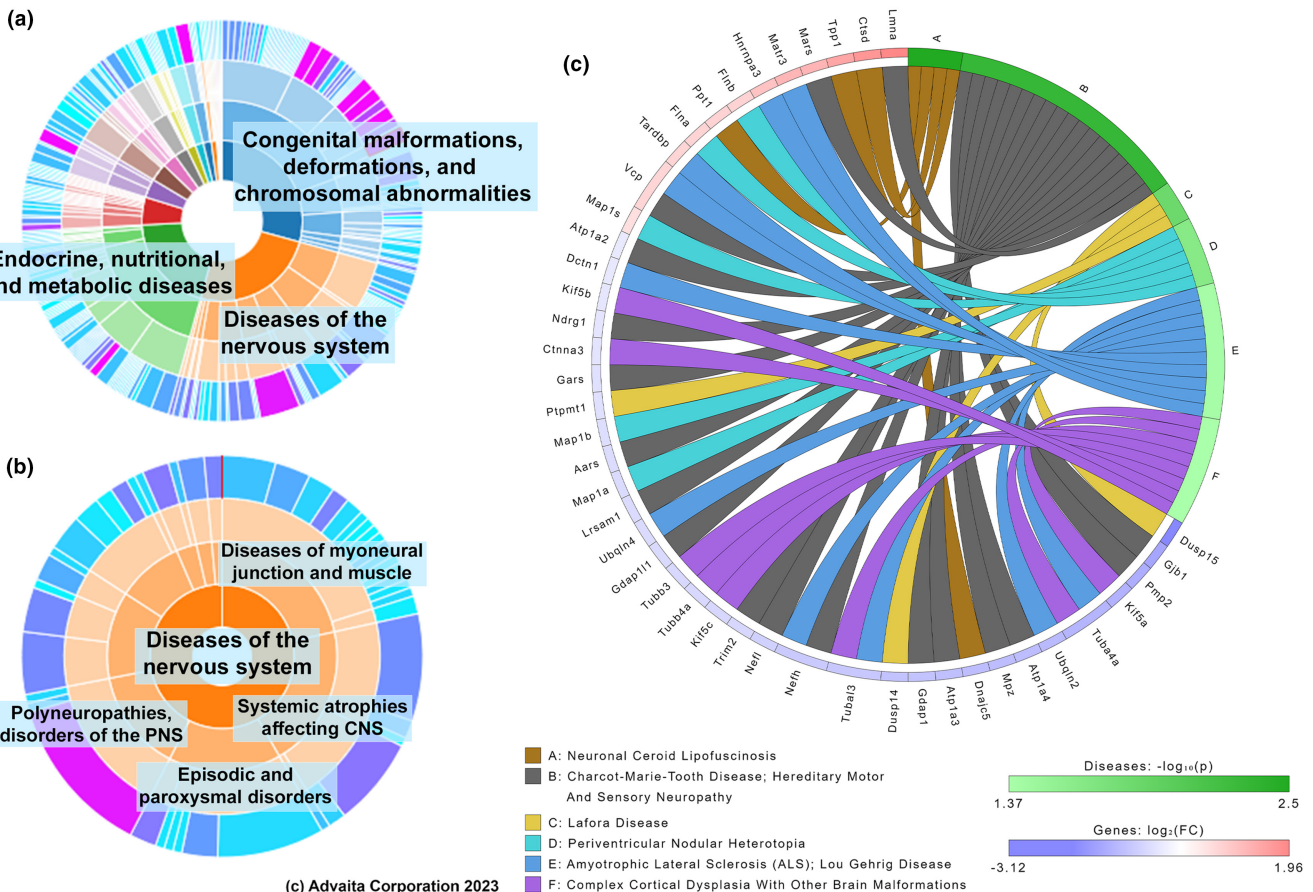


FIGURE 8 Alterations in the neuropathic mouse proteome overlap with previously unrecognized human neurological diseases. (a) Disease summary pie chart map, with the top three clusters noted. (b) The disease summary map of all nervous system disorders from the dataset of significantly enriched protein groups. (c) Chord diagram representing enrichment of nervous system disorders mapped by differentially expressed proteins in TrJ ($n=10$ nerves, from 5 mice) samples, when compared with age-matched Wt ($n=8$ nerves, from 4 mice).

model. While G3BP1 granules cause discrepancies in axonal mRNA translation and nerve regeneration, they can also disturb other cellular functions and signaling (Sahoo et al., 2018). Identification of a well-established marker of axonal disease, G3BP1, substantiates the notion that irrespective of the cellular origin of the neuropathy, the dynamic interplay between the axon and myelinated glia is perturbed early-on in affected nerves.

This unbiased global proteomic study confirms our previous work on the involvement of degradative pathways in PMP22-linked neuropathies (Fortun et al., 2003; Notterpek et al., 1997). Since PMP22, the disease-causing protein, is prone to aggregation when mutated or overexpressed (Notterpek, Ryan, et al., 1999), the mistrafficked protein induces a proteostatic dysbalance (Fortun et al., 2003). Dysregulated proteins identified in this study include autophagy-related cathepsins B, C, D, and Z, lysosomal-associated membrane protein 2, and several other molecules that comprise the lysosome and proteasome pathways (Figures 5 and 6). Recent evidence suggests that the close regulation of autophagy is directly related to the pathobiology of neurodegeneration and is linked to the clearance of intracellular waste in Alzheimer's, Parkinson's, and Huntington's diseases (Song et al., 2021). Upregulation of the

subcellular protein recycling processes, including the proteasome and lysosome, as part of the pathogenic events in neuropathic nerves, is confirmed by this unbiased approach. Macrophage infiltration has also been described in nerves from TrJ mice. At 2 weeks of age, quantitative RT-PCR has detected an increase in inflammatory molecules including Cd40lg, Crp, interleukins and TNF (Okamoto et al., 2013). Morphological studies identified Iba1-positive immune cells in affected nerves from adult TrJ mice (Misko et al., 2002). Our data from the 3-week-old mice is in agreement with these previous publications, as three proteins representing the inflammatory response are significantly altered (Table 2). Nonetheless, as only 3 macrophage specific proteins from the inflammatory response were differentially expressed, it is unlikely that macrophages present within the analyzed nerve tissue contributed significantly to the identified proteomic alterations.

The spliceosome is a highly specialized cellular machine vital for gene expression and correct splicing for further processing into functional proteins. While the spliceosome has been studied in CNS neurological disorders, there is limited information on its involvement in peripheral neuropathies. As mentioned above, the nerve samples analyzed here do not contain neuronal cell bodies; however, they do

include information from the nucleus of glial cells. Significantly, previous studies show that TrJ neuropathy encompasses hyperproliferation of the Schwann cells (Notterpek et al., 1997; Robertson et al., 1997); therefore, a significant fraction of the spliceosome signal likely originates from the glial cells. Diseases involving the spliceosome, termed spliceosomopathies, are known to affect diverse tissues throughout the body (Griffin & Saint-Jeannet, 2020). For example, when the nervous system spliceosome is disturbed, there is a characteristic loss of motor neurons and spinal muscular atrophy, such as in patients with ALS (Beattie & Kolb, 2018; Griffin & Saint-Jeannet, 2020). In our model, based on the tissue analyzed, the amplification in spliceosomal proteins may be due to the higher glial nuclei content of the TrJ mouse sciatic nerve, compared with age-matched Wt.

Neuropathy is a broad term describing a pathological alteration in the nervous system resulting in disease. Peripheral neuropathies comprise a heterogeneous group of neurological disorders with diverse causes, from acute injuries and metabolic disorders to genetic forms. Among the heritable neuropathies, previous studies have mostly focused on the causal genes being glial or neuronal origin. The current examination revealed a previously unrecognized overlap among CMT1E and other neurological disorders (Figure 8). The KEGG database does not explicitly distinguish between type 1 and type 2 CMT neuropathies; however, it correctly labels the TrJ sciatic nerves belonging to that family of diseases. This study uncovered a considerable overlap between known type 2 neuroptotic phenotypes and axonal disturbances within the examined type I, dysmyelinating neuropathy. Furthermore, TrJ nerves show similar defects in proteostatic mechanisms as neuronal ceroid lipofuscinosis and Lafora disease, which are characterized by an accumulation of undegraded waste leading to disease (Naseri et al., 2021; Nitschke et al., 2018). In addition, the similarity of the neuropathic pathology with cytoskeletal and developmental disorders, along with periventricular nodular heterotopia and complex cortical dysplasia (Khoo et al., 2020; Klingler et al., 2021) substantiates previous observations of altered Schwann cell morphology and developmental discrepancies in TrJ nerves (Robertson et al., 1997). Finally, ALS and CMT are known to have similarities in the modifiers responsible for disease heterogeneity (Yamaguchi et al., 2021). Together, these findings support the use of next-generation sequencing for improving the specific diagnosis of neuropathies with shared symptoms and the need for therapies that can benefit distinct forms (Klein, 2020; Okamoto & Takashima, 2023).

In summary, this study provides the first comprehensive proteomic examination of neuropathic nerves from the spontaneous CMT1E mouse model. Notably, we unveiled novel changes in the axonal proteome that are more expansive than the disturbances in myelin proteins. These findings suggest an overlap in subcellular pathology between type 1 and type 2 CMT diseases, paving the way for potential blanket therapeutics. This notion of "blanket therapy" is further corroborated through the parallels of neuropathic mouse nerves with human disorders, ranging from lysosomal storage diseases, cytoskeletal malformation, and motor neuron degeneration. This spontaneous neuropathic mouse model is suitable for investigational therapeutics to benefit distinct neurological illnesses.

AUTHOR CONTRIBUTIONS

Victoria Defilippi: Writing – original draft; methodology; formal analysis; software; investigation. **Juli Peterit:** Investigation; funding acquisition; writing – review and editing; methodology; validation; formal analysis; software; resources. **Valerie J. L. Handlos:** Methodology. **Lucia Notterpek:** Conceptualization; investigation; funding acquisition; methodology; writing – original draft; writing – review and editing; project administration; supervision; resources.

ACKNOWLEDGMENTS

This publication was made possible by grants from the National Institute of General Medical Sciences (GM103440, GM104944, and P20GM130459) from the National Institutes of Health. The Facial Pain Research Foundation and the University of Nevada, Reno, provided additional funds. We thank the Mick Hitchcock, Ph.D. Nevada Proteomics Center ([RRID:SCR_017761](#)) for their involvement in the project. The (LAMP1 rat monoclonal antibody) developed by August, J.T. was obtained from the Developmental Studies Hybridoma Bank, created by the NICHD of the NIH and maintained at The University of Iowa, Department of Biology, Iowa City, IA 52242.

CONFLICT OF INTEREST STATEMENT

The authors declare no conflict of interests.

PEER REVIEW

The peer review history for this article is available at <https://www.webofscience.com/api/gateway/wos/peer-review/10.1111/jnc.16189>.

DATA AVAILABILITY STATEMENT

All relevant data, metadata, and raw files are shared on the data repository Dryad and are identifiable by a unique DOI: <https://doi.org/10.5061/dryad.dbrv15f7t>.

ORCID

Lucia Notterpek  <https://orcid.org/0000-0002-6373-9713>

REFERENCES

- Adinolfi, E., Giuliani, A. L., De Marchi, E., Pegoraro, A., Orioli, E., & Di Virgilio, F. (2018). The P2X7 receptor: A main player in inflammation. *Biochemical Pharmacology*, 151, 234–244.
- Ashburner, M., Ball, C. A., Blake, J. A., Botstein, D., Butler, H., Cherry, J. M., Davis, A. P., Dolinski, K., Dwight, S. S., Eppig, J. T., Harris, M. A., Hill, D. P., Issel-Tarver, L., Kasarskis, A., Lewis, S., Matese, J. C., Richardson, J. E., Ringwald, M., Rubin, G. M., & Sherlock, G. (2000). Gene ontology: Tool for the unification of biology. The gene ontology consortium. *Nature Genetics*, 25, 25–29.
- Beattie, C. E., & Kolb, S. J. (2018). Spinal muscular atrophy: Selective motor neuron loss and global defect in the assembly of ribonucleoproteins. *Brain Research*, 1693, 92–97.
- Chen, Y., Quan, S., Patil, V., Kunjamma, R. B., Tokars, H. M., Leisten, E. D., Joy, G., Wills, S., Chan, J. R., Wong, Y. C., & Popko, B. (2023). Insights into the mechanism of oligodendrocyte protection and remyelination enhancement by the integrated stress response. *Glia*, 71, 2180–2195.



- Cicardi, M. E., Marrone, L., Azzouz, M., & Trott, D. (2021). Proteostatic imbalance and protein spreading in amyotrophic lateral sclerosis. *The EMBO Journal*, 40, e106389.
- Cui, Q., Bi, H., Lv, Z., Wu, Q., Hua, J., Gu, B., Huo, C., Tang, M., Chen, Y., Chen, C., Chen, S., Zhang, X., Wu, Z., Lao, Z., Sheng, N., Shen, C., Zhang, Y., Wu, Z. Y., Jin, Z., ... Bai, G. (2023). Diverse CMT2 neuropathies are linked to aberrant G3BP interactions in stress granules. *Cell*, 186, 803–820.
- de Waegh, S., & Brady, S. T. (1990). Altered slow axonal transport and regeneration in a myelin-deficient mutant mouse: The trembler as an in vivo model for Schwann cell-axon interactions. *The Journal of Neuroscience*, 10, 1855–1865.
- de Waegh, S. M., Lee, V. M., & Brady, S. T. (1992). Local modulation of neurofilament phosphorylation, axonal caliber, and slow axonal transport by myelinating Schwann cells. *Cell*, 68, 451–463.
- DiVincenzo, C., Elzinga, C. D., Medeiros, A. C., Karbassi, I., Jones, J. R., Evans, M. C., Braastad, C. D., Bishop, C. M., Jaremko, M., Wang, Z., Liaquat, K., Hoffman, C. A., York, M. D., Batish, S. D., Lupski, J. R., & Higgins, J. J. (2014). The allelic spectrum of Charcot-Marie-tooth disease in over 17,000 individuals with neuropathy. *Molecular Genetics & Genomic Medicine*, 2, 522–529.
- Ekins, S., Litterman, N. K., Arnold, R. J., Burgess, R. W., Freundlich, J. S., Gray, S. J., Higgins, J. J., Langley, B., Willis, D. E., Notterpek, L., Pleasure, D., Sereda, M. W., & Moore, A. (2015). A brief review of recent Charcot-Marie-tooth research and priorities. *F1000Res*, 4, 53.
- El-Abassi, R., England, J. D., & Carter, G. T. (2014). Charcot-Marie-tooth disease: An overview of genotypes, phenotypes, and clinical management strategies. *PM & R: The Journal of Injury, Function, and Rehabilitation*, 6, 342–355.
- Fortun, J., Dunn, W. A., Joy, S., Li, J., & Notterpek, L. (2003). Emerging role for autophagy in the removal of aggresomes in Schwann cells. *The Journal of Neuroscience*, 23, 10672–10680.
- Fridman, V., & Reilly, M. M. (2015). Inherited neuropathies. *Seminars in Neurology*, 35, 407–423.
- Fridman, V., & Saporta, M. A. (2021). Mechanisms and treatments in demyelinating CMT. *Neurotherapeutics*, 18, 2236–2268.
- Gene Ontology Consortium. (2001). Creating the gene ontology resource: design and implementation. *Genome Research*, 11, 1425–1433.
- Gillet, L. C., Navarro, P., Tate, S., Röst, H., Selevsek, N., Reiter, L., Bonner, R., & Aebersold, R. (2012). Targeted data extraction of the MS/MS spectra generated by data-independent acquisition: A new concept for consistent and accurate proteome analysis. *Molecular & Cellular Proteomics*, 11(O111), 16717.
- Griffin, C., & Saint-Jeanet, J. P. (2020). Spliceosomopathies: Diseases and mechanisms. *Developmental Dynamics*, 249, 1038–1046.
- Hildebrand, A., Schreiber, F., Weber, L., Arndt, P., Garz, C., Petri, S., Prudlo, J., Meuth, S. G., Waerzeggers, Y., Henneicke, S., Vielhaber, S., & Schreiber, S. (2023). Peripheral nerve ultrasound for the differentiation between ALS, inflammatory, and hereditary polyneuropathies. *Medicina*, 59, 1–11.
- Hoch-Kraft, P., Trotter, J., & Gonsior, C. (2020). Missing in action: Dysfunctional RNA metabolism in Oligodendroglial cells as a contributor to neurodegenerative diseases? *Neurochemical Research*, 45, 566–579.
- Hong, J., Garfolo, R., Kabre, S., Humml, C., Velanac, V., Roue, C., Beck, B., Jeanette, H., Haslam, S., Bach, M., Arora, S., Acheta, J., Nave, K. A., Schwab, M. H., Joud'heuil, D., Poitelon, Y., & Belin, S. (2024). PMP2 regulates myelin thickening and ATP production during remyelination. *Glia*, 72, 885–898.
- Hong, Y. B., Joo, J., Hyun, Y. S., Kwak, G., Choi, Y. R., Yeo, H. K., Jwa, D. H., Kim, E. J., Mo, W. M., Nam, S. H., Kim, S. M., Yoo, J. H., Koo, H., Park, H. T., Chung, K. W., & Choi, B. O. (2016). A mutation in PMP2 causes dominant demyelinating Charcot-Marie-tooth neuropathy. *PLoS Genetics*, 12, e1005829.
- Hoyer, H. L., Busk, Ø., Esbensen, Q. Y., Røsby, O., Hilmarsen, H. T., Russell, M. B., Nyman, T. A., Braathen, G. J., & Nilsen, H. L. (2022). Clinical characteristics and proteome modifications in two Charcot-Marie-tooth families with the AARS1 Arg326Trp mutation. *BMC Neurology*, 22, 299.
- Kanehisa, M. (2002). The KEGG database. *Novartis Foundation Symposium*, 247, 91–101. discussion 101–103, 119–128, 244–152.
- Kanehisa, M., & Goto, S. (2000). KEGG: Kyoto encyclopedia of genes and genomes. *Nucleic Acids Research*, 28, 27–30.
- Karamysheva, Z., Diaz-Martinez, L. A., Warrington, R., & Yu, H. (2015). Graded requirement for the spliceosome in cell cycle progression. *Cell Cycle*, 14, 1873–1883.
- Khajavi, M., Shiga, K., Wiszniewski, W., He, F., Shaw, C. A., Yan, J., Wensel, T. G., Snipes, G. J., & Lupski, J. R. (2007). Oral curcumin mitigates the clinical and neuropathologic phenotype of the trembler-J mouse: A potential therapy for inherited neuropathy. *American Journal of Human Genetics*, 81, 438–453.
- Khoo, H. M., Gotman, J., Hall, J. A., & Dubeau, F. (2020). Treatment of epilepsy associated with periventricular nodular heterotopia. *Current Neurology and Neuroscience Reports*, 20, 59.
- Klein, C. J. (2020). Charcot-Marie-tooth disease and other hereditary neuropathies. *Continuum*, 26, 1224–1256.
- Klingler, E., Francis, F., Jabaudon, D., & Cappello, S. (2021). Mapping the molecular and cellular complexity of cortical malformations. *Science*, 371, 1–33.
- Koppenol, R., Conceição, A., Afonso, I. T., Afonso-Reis, R., Costa, R. G., Tomé, S., Teixeira, D., da Silva, J. P., Côdesso, J. M., Brito, D. V. C., Mendonça, L., Marcelo, A., Pereira de Almeida, L., Matos, C. A., & Nóbrega, C. (2023). The stress granule protein G3BP1 alleviates spinocerebellar ataxia-associated deficits. *Brain*, 146, 2346–2363.
- Krainer, J., Siebenhandl, S., & Weinhäusel, A. (2020). Systemic autoinflammatory diseases. *Journal of Autoimmunity*, 109, 102421.
- Lee, J. S., Chang, E. H., Koo, O. J., Jwa, D. H., Mo, W. M., Kwak, G., Moon, H. W., Park, H. T., Hong, Y. B., & Choi, B. O. (2017). Pmp22 mutant allele-specific siRNA alleviates demyelinating neuropathic phenotype in vivo. *Neurobiology of Disease*, 100, 99–107.
- Li, Y., Zeng, H., Wei, Y., Ma, X., & He, Z. (2023). An overview of the therapeutic strategies for the treatment of spinal muscular atrophy. *Human Gene Therapy*, 34, 180–191.
- Madorsky, I., Opalach, K., Waber, A., Verrier, J. D., Solmo, C., Foster, T., Dunn, W. A., & Notterpek, L. (2009). Intermittent fasting alleviates the neuropathic phenotype in a mouse model of Charcot-Marie-tooth disease. *Neurobiology of Disease*, 34, 146–154.
- Misko, A., Ferguson, T., & Notterpek, L. (2002). Matrix metalloproteinase mediated degradation of basement membrane proteins in trembler J neuropathy nerves. *Journal of Neurochemistry*, 83, 885–894.
- Mitra, S., Gumusgoz, E., & Minassian, B. A. (2022). Lafora disease: Current biology and therapeutic approaches. *Revue Neurologique (Paris)*, 178, 315–325.
- Motley, W. W., Palaima, P., Yum, S. W., Gonzalez, M. A., Tao, F., Wanschitz, J. V., Strickland, A. V., Loscher, W. N., De Vriendt, E., Koppi, S., Medne, L., Janecke, A. R., Jordanova, A., Zuchner, S., & Scherer, S. S. (2016). De novo PMP2 mutations in families with type 1 Charcot-Marie-tooth disease. *Brain*, 139, 1649–1656.
- Msheik, Z., Durand, S., Pinault, E., Caillaud, M., Vignaud, L., Billet, F., El Massry, M., & Desmouliere, A. (2023). Charcot-Marie-tooth-1A and sciatic nerve crush rat models: Insights from proteomics. *Neural Regeneration Research*, 18, 1354–1363.
- Napolitano, G., & Ballabio, A. (2016). TFEB at a glance. *Journal of Cell Science*, 129, 2475–2481.
- Naseri, N., Sharma, M., & Velinov, M. (2021). Autosomal dominant neuronal ceroid lipofuscinosis: Clinical features and molecular basis. *Clinical Genetics*, 99, 111–118.
- Nicks, J., Lee, S., Harris, A., Falk, D. J., Todd, A. G., Arredondo, K., Dunn, W. A., & Notterpek, L. (2014). Rapamycin improves peripheral nerve myelination while it fails to benefit neuromuscular performance in neuropathic mice. *Neurobiology of Disease*, 70, 224–236.

- Nitschke, F., Ahonen, S. J., Nitschke, S., Mitra, S., & Minassian, B. A. (2018). Lafora disease - from pathogenesis to treatment strategies. *Nature Reviews. Neurology*, 14, 606–617.
- Notterpek, L., Ryan, M. C., Tobler, A. R., & Shooter, E. M. (1999). PMP22 accumulation in aggresomes: Implications for CMT1A pathology. *Neurobiology of Disease*, 6, 450–460.
- Notterpek, L., Shooter, E. M., & Snipes, G. J. (1997). Upregulation of the endosomal-lysosomal pathway in the trembler-J neuropathy. *The Journal of Neuroscience*, 17, 4190–4200.
- Notterpek, L., Snipes, G. J., & Shooter, E. M. (1999). Temporal expression pattern of peripheral myelin protein 22 during in vivo and in vitro myelination. *Glia*, 25, 358–369.
- Notterpek, L., & Tolwani, R. J. (1999). Experimental models of peripheral neuropathies. *Laboratory Animal Science*, 49, 588–599.
- Nita, D. A., Mole, S. E., & Minassian, B. A. (2016). Neuronal ceroid lipofuscinosis. *Epileptic Disorders*, 18(s2), 73–88. <https://doi.org/10.1684/epd.2016.0844>
- Okamoto, Y., Pehlivan, D., Wiszniewski, W., Beck, C. R., Snipes, G. J., Lupski, J. R., & Khajavi, M. (2013). Curcumin facilitates a transitory cellular stress response in trembler-J mice. *Human Molecular Genetics*, 22, 4698–4705.
- Okamoto, Y., & Takashima, H. (2023). The current state of Charcot-Marie-tooth disease treatment. *Genes*, 14, 1–17.
- Robertson, A. M., King, R. H., Muddle, J. R., & Thomas, P. K. (1997). Abnormal Schwann cell/axon interactions in the trembler-J mouse. *Journal of Anatomy*, 190(Pt 3), 423–432.
- Sahoo, P. K., Kar, A. N., Samra, N., Terenzio, M., Patel, P., Lee, S. J., Miller, S., Thamess, E., Jones, B., Kawaguchi, R., Coppola, G., Fainzilber, M., & Twiss, J. L. (2020). A Ca(2+)-dependent switch activates axonal casein kinase 2α translation and drives G3BP1 granule disassembly for axon regeneration. *Current Biology*, 30, 4882–4895.e4886.
- Sahoo, P. K., Lee, S. J., Jaiswal, P. B., Alber, S., Kar, A. N., Miller-Randolph, S., Taylor, E. E., Smith, T., Singh, B., Ho, T. S., Urisman, A., Chand, S., Pena, E. A., Burlingame, A. L., Woolf, C. J., Fainzilber, M., English, A. W., & Twiss, J. L. (2018). Axonal G3BP1 stress granule protein limits axonal mRNA translation and nerve regeneration. *Nature Communications*, 9, 3358.
- Sakakura, M., Hadziselimovic, A., Wang, Z., Schey, K. L., & Sanders, C. R. (2011). Structural basis for the trembler-J phenotype of Charcot-Marie-tooth disease. *Structure*, 19, 1160–1169.
- Saporta, A. S., Sottile, S. L., Miller, L. J., Feely, S. M., Siskind, C. E., & Shy, M. E. (2011). Charcot-Marie-tooth disease subtypes and genetic testing strategies. *Annals of Neurology*, 69, 22–33.
- Siems, S. B., Jahn, O., Eichel, M. A., Kannaiyan, N., Wu, L. M. N., Sherman, D. L., Kusch, K., Hesse, D., Jung, R. B., Fledrich, R., Sereda, M. W., Rossner, M. J., Brophy, P. J., & Werner, H. B. (2020). Proteome profile of peripheral myelin in healthy mice and in a neuropathy model. *eLife*, 9, 1–31.
- Snipes, G. J., Suter, U., Welcher, A. A., & Shooter, E. M. (1992). Characterization of a novel peripheral nervous system myelin protein (PMP-22/SR13). *The Journal of Cell Biology*, 117, 225–238.
- Song, T. T., Cai, R. S., Hu, R., Xu, Y. S., Qi, B. N., & Xiong, Y. A. (2021). The important role of TFEB in autophagy-lysosomal pathway and autophagy-related diseases: A systematic review. *European Review for Medical and Pharmacological Sciences*, 25, 1641–1649.
- Suter, U., Welcher, A. A., Ozcelik, T., Snipes, G. J., Kosaras, B., Francke, U., Billings-Gagliardi, S., Sidman, R. L., & Shooter, E. M. (1992). Trembler mouse carries a point mutation in a myelin gene. *Nature*, 356, 241–244.
- Taveggia, C., & Feltri, M. L. (2022). Beyond wrapping: Canonical and non-canonical functions of Schwann cells. *Annual Review of Neuroscience*, 45, 561–580.
- Tobler, A. R., Notterpek, L., Naef, R., Taylor, V., Suter, U., & Shooter, E. M. (1999). Transport of trembler-J mutant peripheral myelin protein 22 is blocked in the intermediate compartment and affects the transport of the wild-type protein by direct interaction. *The Journal of Neuroscience*, 19, 2027–2036.
- Valentijn, L. J., Baas, F., Wolterman, R. A., Hoogendoijk, J. E., van den Bosch, N. H., Zorn, I., Gabreels-Festen, A. W., de Visser, M., & Bolhuis, P. A. (1992). Identical point mutations of PMP-22 in trembler-J mouse and Charcot-Marie-tooth disease type 1A. *Nature Genetics*, 2, 288–291.
- van Paassen, B. W., van der Kooi, A. J., van Spaendonck-Zwarts, K. Y., Verhamme, C., Baas, F., & de Visser, M. (2014). PMP22 related neuropathies: Charcot-Marie-tooth disease type 1A and hereditary neuropathy with liability to pressure palsies. *Orphanet Journal of Rare Diseases*, 9, 38.
- Yamaguchi, M., Omori, K., Asada, S., & Yoshida, H. (2021). Epigenetic regulation of ALS and CMT: A lesson from drosophila models. *International Journal of Molecular Sciences*, 22, 1–19.
- Yim, A. K. Y., Wang, P. L., Birmingham, J. R., Hackett, A., Strickland, A., Miller, T. M., Ly, C., Mitra, R. D., & Milbrandt, J. (2022). Disentangling glial diversity in peripheral nerves at single-nuclei resolution. *Nature Neuroscience*, 25, 238–251.
- Yoshimi, A., & Abdel-Wahab, O. (2017). Molecular pathways: Understanding and targeting mutant Spliceosomal proteins. *Clinical Cancer Research*, 23, 336–341.
- Zhou, Y., Bazick, H., Miles, J. R., Fethiere, A. I., Salihi, M. O. A., Fazio, S., Tavori, H., & Notterpek, L. (2019). A neutral lipid-enriched diet improves myelination and alleviates peripheral nerve pathology in neuropathic mice. *Experimental Neurology*, 321, 113031.
- Zhou, Y., Borchelt, D., Bauson, J. C., Fazio, S., Miles, J. R., Tavori, H., & Notterpek, L. (2020). Subcellular diversion of cholesterol by gain- and loss-of-function mutations in PMP22. *Glia*, 68, 2300–2315.
- Zhou, Y., & Notterpek, L. (2016). Promoting peripheral myelin repair. *Experimental Neurology*, 283, 573–580.

How to cite this article: Defilippi, V., Petereit, J., Handlos, V. J. L., & Notterpek, L. (2024). Quantitative proteomics unveils known and previously unrecognized alterations in neuropathic nerves. *Journal of Neurochemistry*, 168, 3154–3170. <https://doi.org/10.1111/jnc.16189>